Techno-Economic Analysis of a Concentrating Solar Power Plant

Using Reduction/Oxidation Metal Oxides for Thermochemical Energy Storage

by

Mariana Lopes

A Thesis Presented in Partial Fulfillment
of the Requirements for the Degree
Master of Science

Approved June 2017 by the
Graduate Supervisory Committee:

Nathan Johnson, Chair
Ellen Stechel
Paul Westerhoff

ARIZONA STATE UNIVERSITY

August 2017

ABSTRACT

Concentrating Solar Power (CSP) plant technology can produce reliable and dispatchable electric power from an intermittent solar resource. Recent advances in thermochemical energy storage (TCES) can offer further improvements to increase off-sun operating hours, improve system efficiency, and the reduce cost of delivered electricity. This work describes a 111.7 MWe CSP plant with TCES using a mixed ionic-electronic conducting metal oxide, CAM28, as both the heat transfer and thermal energy storage media. Turbine inlet temperatures reach 1200 °C in the combined cycle power block. A techno-economic model of the CSP system is developed to evaluate design considerations to meet targets for low-cost and renewable power with 6-14 hours of dispatchable storage for off-sun power generation. Hourly solar insolation data is used for Barstow, California, USA. Baseline design parameters include a 6-hour storage capacity and a 1.8 solar multiple. Sensitivity analyses are performed to evaluate the effect of engineering parameters on total installed cost, generation capacity, and levelized cost of electricity (LCOE). Calculated results indicate a full-scale 111.7 MWe system at $274 million in installed cost can generate 507 GWh per year at a levelized cost of $0.071 per kWh. Expected improvements to design, performance, and costs illustrate options to reduce energy costs to less than $0.06 per kWh.

ACKNOWLEDGMENTS

I am thankful for my advisor, Prof. Nathan Johnson for providing me with intellectual assistance, learning opportunities and networking in the academic community and look forward to our future collaborations.

I want to thank Dr. Ellen Stechel for sharing her knowledge with me and assisting me along the way, and for the great conversations and insights.

I also want to thank Prof. Paul Westerhoof for his time, intellect and resources that allowed me to complete this project.

This work was partially funded by NSF IGERT-SUN program at Arizona State University and is part of a larger project entitled "High Performance Reduction/Oxidation Metal Oxides for Thermochemical Energy Storage" (PROMOTES) funded as a subcontractor to Sandia National Laboratories through the Department of Energy (DOE) SunShot initiative within the ELEMENTS portfolio under award number DE-FOA-0000805-1541.

The authors would like to thank all the members of the PROMOTES team for useful conversations and insights, including Prof. Hany Al Ansari, Dr. Jim Miller Dr. Andrea Ambrosini, Dr. Sean Babiniec, Dr. Eric Coker, Dr. Cliff Ho, Prof. Sheldon Jeter, Prof. Peter Loutzenheiser, Andrew Shrader, and Brandon Gorman. The authors would like to recognize Rob Stirling as he guided us on the general structure, some of the fits, and the method of using the setting, piping, and electrical multipliers.

Sandia is a multiprogramming laboratory operated by Sandia Corporation, a Lockheed Martin Company, for the United States Department of Energy's National Nuclear Security Administration under contract DE-AC04-94AL85000.

TABLE OF CONTENTS

LIST OF TABLES

LIST OF FIGURES

GENERAL NOMENCLATURE

Nomenclature	Units	Description
$\Delta\dot{E}_{SR3}$	W	SR3 Energy Balance
$\dot{Q}_2$	W	Energy of particles into the SR3
$\dot{E}_1$	W	Energy of particles into the SR3
$\dot{E}_4$	W	Energy of particles into the HS
$\dot{E}_5$	W	Energy of oxygen out of SR3
$\dot{Q}_{18}$	W	SR3 energy loss
E_{HS}	J	HS energy loss
E_{22}	J	Energy of nitrogen stream into of HS
E_{23}	J	Energy of nitrogen stream out of HS
$\dot{n}_n$	moles	Moles of nitrogen
$\bar{c}_{p,n}$	J/mol	Specific heat of nitrogen
T_{22}	k	Temperature of nitrogen into HS
T_{23}	k	Temperature of nitrogen out of HS
$\Delta\dot{E}_{ROx}$	W	Energy balance of ROx
$\dot{E}_9$	W	Energy of oxygen into the ROx
$\dot{E}_{11}$	W	Energy of oxygen out of the ROx and into the power block
$\dot{E}_7$	W	Energy of particles into the ROx
$\dot{E}_{10}$	W	Energy of particles into the cold storage
$\dot{Q}_{17}$	W	Energy loss from ROx
E_{CS}	J	Energy balance of cold storage
E_{13}	J	Energy of particles out of the cold storage
Q_{14}	J	Cold storage heat loss
$[\dot{n}_p]_{7,10}$	mol/s	Particle flow through ROx
$[\dot{n}_p]_{1,4,13}$	mol/s	Particle flow through SR3
$\dot{E}_{HX}$	W	Energy balance of heat exchanger
$\dot{E}_3$	W	Energy of oxygen out of the heat exchanger
$\dot{Q}_{19}$	W	Heat exchanger energy loss
$\dot{E}_{pump}$	W	Energy balance of the pump
$\dot{n}_{O_2}$	mol/s	Molar flow of oxygen through the pump
T_0	k	Ambient temperature
p_{amb}	atm	Ambient Pressure
p_{sr3}	atm	SR3 oxygen pressure
η_{pu}	%	Pump efficiency
$\dot{n}_{air}$	mol/s	Air flow through the ROx
$\bar{c}_{p,air,}$	J/mol	Specific heat of air
T_{11}	k	Temperature of air out of the power block
T_9	k	Temperature of into the power block
CF	/	Concentration factor
A_a	M^2	Area of the SR3 apparatus
$\dot{J}_{DNI}$	W/m^2	Incident direct normal radiance
$\bar{C}_{p,p}$	J/mol	Specific heat of the particles
T_4	k	Temperature of the particles out of the SR3
δ	/	Particle extent of reduction
t_{st}	hr	Storage hours

CHAPTER 1

INTRODUCTION

Global energy demand is estimated to grow by more than 30% by 2040 with the share of renewables will increasing from 15% to 37% over the same period due to decreasing costs, rising societal interest in clean energy, and political mandates (World Energy Outlook 2016). Recent decreases in the installed cost of solar photovoltaics (PV) and wind power, coupled with subsidies and tax incentives in some countries, have favored the installation of theses renewables over other alternatives (Boekhoudt and Behrendt 2014; Energy Policy Act 2005; Sawin et al. 2016; Durkay 2016; World Energy Council 2010). Yet progress towards cleaner power has not come without challenge or difficulty. High-penetration uncontrolled solar PV and wind generation can stress electrical infrastructure and upset traditional utility business models (California ISO 2013; U.S. Department of Energy 2015b; Janko et al. 2016; Thongpron et al. 2004; Wirth 2015; U.S. Department of Energy 2009 add). Energy storage is one way to mitigate the negative effects of intermittency renewables and can provide utilities with a dispatchable resource for peak power or operating reserve (Eber and Corbus 2013; U.S. Federal Energy Regulatory Commission 2012; Germany Federal Ministry for Economic Affairs and Energy 2014; Jamehbozorg et al. 2011; Lam and Yeh 2014; Wang et al. 2014).

Common forms of storage include pumped hydropower, batteries, capacitors, flywheels, and thermal storage (Boucher and Rodzianko 1994; Garg et al. 1985; Lieurance et al. 1995). Thermal energy storage is increasingly used with concentrating solar power (CSP) plants as a means to mitigate solar intermittency and expand plant operating hours into the evening, thereby increasing the value of CSP to the grid (Thomas and Guven,

1993; Price 2001; Price 1997; Price 2000; Cohen et al. 1999; Duke Solar Energy 2001). The resulting increase in plant capacity factor can, in turn, decrease the levelized cost of electricity (LCOE) by increasing productivity at a higher rate than cost, up to a point that a minimum LCOE is reached. CSP coupled with storage has been found to achieve a lower LCOE than solar PV plus batteries, even with a reduction in battery price (Jorgenson et al. 2016; Boudaoud et al. 2015). Further improvement in CSP performance is extended through emerging technologies and evaluating the effect of engineering and cost parameters on productivity and LCOE (Charles et al., 2005).

This study describes a 111.7 MWe CSP system and supporting techno-economic analysis to provide low-cost, renewable power with 6-14 hours of dispatchable storage for off-sun power generation. A mixed ionic-electronic conducting metal oxide, CAM28, is used as both the heat transfer and thermal energy storage media. Baseline design parameters include 6-hour storage capacity and 1.8 solar multiple. Productivity is calculated over a one-year period with hourly solar insolation data taken for Barstow, California, USA. Sensitivity analyses are performed to evaluate the effect of engineering and cost parameters on total installed cost, generation capacity, and LCOE. Calculated performance characteristics are given for the full-scale 111.7 MWe system with expected improvements to design, performance, and costs enumerated to reach LCOE targets less than $0.06 per kWh.

CHAPTER 2
BACKROUND

CSP plants use heat transfer fluids (HTFs) to absorb radiant energy in a solar receiver and transfer that energy to a power block, or to intermediate storage, to generate power. Examples of HTFs include steam, oil, molten salts, liquid metals, and phase changing materials (PCM). Steam is limited to operating at below 600 °C and cannot serve as thermal storage. Thermal oils and molten salts are common materials used as thermal energy storage and HTF, but each they thermally stable only to 400 °C, and 600 °C respectively. Liquid metals are stable at higher temperatures above 1000 °C but have high corrosion and a high cost of operation (Lorenzin and Abánades 2016; Pacio et al. 2013). PCM tend to have higher energy density (gravimetric and volumetric) than sensible heat only materials due to the additional energy in latent heat capacity (Glatzmaier, 2011). However, PCMs have not replaced synthetic oils or molten salts in linear concentrating or power tower applications due to the low power density of commercially available PCMs that limit the rate of heat transfer and performance of the power block. PCM have shown promise for Dish–Stirling Engine applications because of the lower temperature requirements and because heat transfer from the material to the engine is isothermal and occurs simultaneously with the heat transfer of the sun to the material (Shabgard et al., 2014; Sharifi et al., 2015). High temperature materials are prefered as they result in higher Carnot efficiencies with the ability to use a combined-cycle systems.

Emerging research in materials that undergo reversible thermochemical reactions can be used as both the HTF and energy storage media (Pena and Fierro 2001). A redox active metal oxide operates in a two-step thermochemical cycle: reduction when the

material heats in a solar receiver and re-oxidization upon exposure to oxygen (in air). Such a material can be stored at elevated temperatures in a reduced form and then exposed to air on demand to produce dispatchable electric power. Recent experiments have shown that air temperatures as high as 1200 °C can be reached from the exothermic reaction (Babiniec et al 2016) providing an opportunity for using higher-efficiency combined cycle engines with greater power output.

2.1 Redox Active Material

Perovskite (ABO_{3-x}) metal oxides were chosen as the mixed ionic-electronic conducting (MIEC) materials in this study. Metal oxides with MIEC properties offer faster reduction and re-oxidation kinetics than non-conducting metal oxides, are tunable over a large parameter space (which allows for specific thermodynamic properties to be optimized), and do not undergo major structural rearrangements during re-oxidation or reduction (Miller et al. 2014). Further benefits of MIEC materials are that redox reactions are not limited to the material surface and materials are physically stable at elevated temperatures (Pardo et al. 2014). The thermochemical and kinetic properties of metal oxides with MIEC properties offer transformative potential in CSP systems with energy storage and higher-temperature power cycles with greater efficiency and power output.

The stoichiometric balance for reduction and re-oxidation of the perovskite metal oxide is shown in Eq. 2.1 where oxygen is the only additional product and reactant. The reduction extent of this instantaneous reaction, symbolized by δ, is a function of the working temperature, partial pressure of oxygen, and the specific perovskite material. The extent of reduction increases at higher temperatures and lower pressures, which is limited

by the performance of the vacuum pump. The specific material used here is $CaAl_{0.2}Mn_{0.8}O_{2.9}$ (CAM28) and has been experimentally measured and characterized by Sandia National Laboratories (Babiniec et al. 2016).

$$\frac{1}{\delta}\, ABO_{3-\mathrm{X}} \leftrightarrow \frac{1}{\delta}\, ABO_{3-x-\delta} + \frac{1}{2} O_{2(\mathrm{g})} \tag{2.1}$$

CHAPTER 3

THERMODYNAMIC MODEL DEVELOPMENT

The schematic in Fig. 1 shows major energy and mass flows of the CSP system integrated with TCES. Metal oxide particles circulate within a closed system whereas the air Brayton power block operates as an open system. Figure 2 provides state information and stream flows with representative temperatures for design point operation at 900 W/m^2 developed in other work (Gorman et al. 2017).

The particle loop beings with the Solar Receiver Reducing Reactor (SR3) that receives concentrated sunlight from the solar field to heat and drive the endothermic reduction reaction of the metal oxide media. The hot storage (HS) charges with reduced particles during sunlight hours and discharges in off-sun hours to provide dispatchable power. Hot reduced particles pass through the ROx, mix directly with pressurized air to exchange sensible energy, and extract oxygen from air yielding an exothermic chemical reaction that creates a rise in temperature the air outlet temperature to a value greater than the particle inlet temperature. Cooled, re-oxidized, particles then enter the cold storage (CS) hopper until they can be reheated during on-sun hours of the day. A heat exchanger (HX) at the top of the tower acts as a recuperator to preheat particles using the waste heat from oxygen extracted from particles in the SR3.

Other components in the full-scale system include a vacuum pump to maintain the target oxygen partial pressure in the SR3, the power block, a nitrogen pump connected to the HS to prevent particle re-oxidation from exposure to air, and the solar field that focuses solar radiation into the SR3.

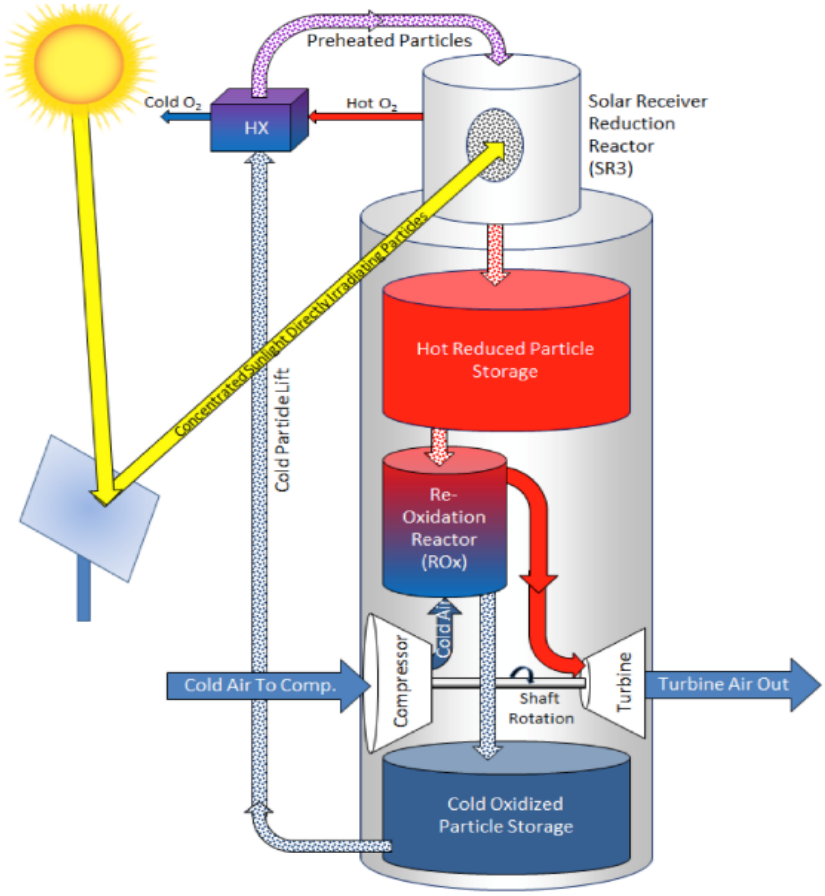

Figure 1. Component Diagram of CSP System Showing Major Energy and Mass Flows

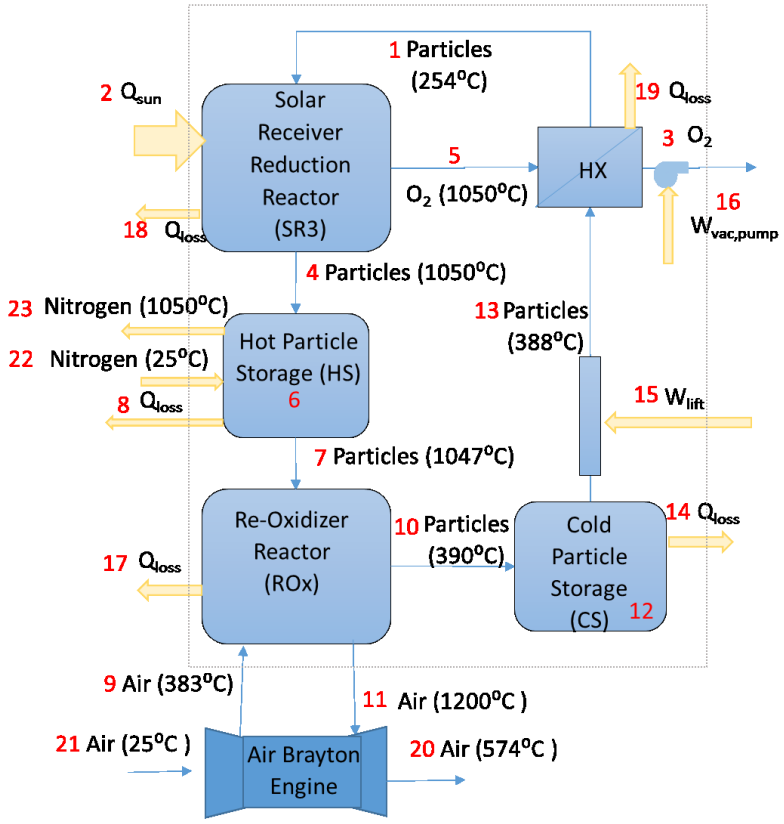

Figure 2. Component and Flow Diagram for the PROMOTES System with Representative Temperatures.

3.1 Thermodynamic Equation Set

Thermodynamic equations for the quasi-steady state energy balance for each component are given in Table 1. Data for the Barstow solar radiation was taken from National Renewable Energy Laboratories (National Renewable Energy Laboratory n.d). Understanding that $\dot{E}_4 = \left[\dot{n}_p\right]_{1,4,13} \cdot (\bar{C}_{p,p} \cdot (T_4 - T_1) + \frac{\delta}{2} \cdot \Delta\bar{H}_{rxn})$, where the heat capacity, $\bar{C}_{p,p}$, and the enthalpy of reduction per oxygen molecule, $\Delta\bar{H}_{rxn}$, are approximated as constants as illustrated in Table 1. Energy losses from the receiver, $\dot{Q}_{18}$, include re-radiation, convection, and conduction losses. The extent of reduction is equated

to be $\delta = 0.205$ as a function of experimental observations of CAM28 materials, a reduction temperature 1050 °C, and an oxygen partial pressure of 200 Pa. Equation 3.1 provides the fit obtained through thermal gravimetric analysis (TGA).

$$\delta = e^{-\left(\frac{7.49697-10.7886\cdot\chi+6.68975\cdot(e^{\chi}-1.0-\chi)-0.292324\cdot u+0.319622\cdot\chi\cdot u}{1.0+0.104546}\right)} - .000574 \quad (3.1)$$

Where χ is a function of temperature, and u a function of pressure as indicated in Equations (3.4-3.7). The fit was solved self-consistently and assumes that δ=0 at u=0 and β=1. Note that the β term and u term is normalized to 298.15 K and 0.20946 atm, respectively. T_4 is the temperature of the par m²ticles leaving the SR3, and p_{O_2} is the partial pressure of oxygen in the SR3.

$$\chi \equiv Ln\left[\frac{298.15}{T_4}\right] = -Ln[\beta] \quad (3.2)$$

$$u \equiv \frac{1}{2}Ln[\frac{20946}{p_{O_2}}] \quad (3.3)$$

Table 1. Thermodynamic Equation Set

Component	Energy Balance	Comments
SR3	$\Delta\dot{E}_{SR3} = \dot{Q}_2 + \dot{E}_1 - \dot{E}_4 - \dot{E}_5 - \dot{Q}_{18}$	Continuous particle flow through the SR3 absorbs the energy from the solar field ($\dot{Q}_2$) and both heats and reduces the entering particle stream. Particles and oxygen exit. Main losses are due to re-radiation conduction through the main body and insulation and convection by the ambient air. Convective losses depend on the total aperture area.
Hot Storage	$E_{HS}^{t} = E_{HS}^{t-1} + \Delta E_{HS} = E_{HS}^{t-1} + E_4^{t-1} - E_7^{t-1} - Q_8^{t-1} + E_{22}^{t-1} - E_{23}^{t-1}$	The loss from hot storage is due to convective losses due to the nitrogen and stored particles. This loss (<1%) affects particles leaving the hopper and the stored energy.
Nitrogen pump	$E_{22}^{t-1} - E_{23}^{t-1} = [\dot{n}_n]\bar{c}_{p,n} \cdot (T_{22} - T_{23})$	The moles of nitrogen inserted into the bin contribute to a change in energy in the bin and is dependent on the subtraction of the total volume of the hopper and the volume of the particles.

ROx	$\Delta\dot{E}_{ROx} = \dot{E}_9 - \dot{E}_{11} + \dot{E}_7 - \dot{E}_{10} - \dot{Q}_{17}$	Counter-current quasi steady-state energy balance about the ROx hot reduced particles and compressed air in, cooled oxidized particles and hot air out. The heat loss is due to convection to insulation, conduction through insulation, and convection to ambient air. The total convective losses depend on the number of ROx pipes.
Cold Storage	$E_{CS}^{t} = E_{CS}^{t-1} + \Delta = E_{CS}^{t-1} + E_{10}^{t-1} - E_{13}^{t-1} - Q_{14}^{t-1} + E_{24}^{t-1} - E_{25}^{t-1}$	The cold storage is charged or discharged based on $\left[\dot{n}_p\right]_{7,10}$ and $\left[\dot{n}_p\right]_{1,4,13}$. Heat losses in the cold storage are due to convective losses by the stored air and conductive losses due to the particles.
HX	$\Delta\dot{E}_{HX} = 0 = \dot{E}_5 + \dot{E}_{13} - \dot{E}_1 - \dot{E}_3 - \dot{Q}_{19}$	The sensible heat in the oxygen (stream 5) is used to calculate the energy balance of the heat exchanger. The equation uses the number of transfer units (NTU) method to calculate the effectiveness of a counter-current flow heat exchanger.
Vacuum Pump	$\Delta\dot{E}_{pump} = \left[\dot{n}_{O_2}\right]_5 \cdot \mathrm{R} \cdot T_0 \cdot \log(\frac{p_{amb}}{p_{sr3}})/\eta_{\mathrm{pu}}$	The energy for the vacuum pump is dependent on the moles of oxygen needed to evacuate and the partial pressure differential between the ambient and the SR3.
Power Block	$\dot{E}_{11} - \dot{E}_9 = [\dot{n}_{air}] \cdot \bar{c}_{p,air,} \cdot (T_{11} - T_9)$	Temperatures and pressures are based on specification from the manufacturer (Turbomachinery Handbook, 2015).
Solar Field	$\Delta\dot{Q}_2 = CF \cdot A_a \cdot \dot{I}_{DNI}$	The reflected by the solar field into the receiver is dependent on the total size of the field and the DNI incident on the field.

Particle flow rate through the SR3 is calculated based on selected state temperatures, extent of reduction, radiation entering the receiver, and heat loss as given in Eq. 3.1. Higher reduction extents decrease particle flow rate for the same electrical generation because energy density increases due to the rise in thermochemical potential. This benefit is not without bound, however, because of additional energy needed for the vacuum pump and limitations in component integrity under very low particle pressures.

$$\left[\dot{n}_p\right]_{1,4,13} = \frac{\dot{Q}_2 - \dot{Q}_{18}}{\bar{c}_{p,p} \cdot (T_4 - T_1) + \frac{\delta}{2} \cdot \Delta\bar{H}_{rxn}} \tag{3.4}$$

The instantaneous amount of particles in hot storage is calculated using the previous amount in storage, charging rate, and discharging rate. Stored particles experience a modest temperature drop while hot storage due to heat loss through the hopper walls. Nitrogen is

pumped into the HS to prevent undesired oxidization. ROx heat loss, $\dot{Q}_{17}$, is based on the surface area of the ROx. The flow rate of the particles needed to heat air to the specified temperature is calculated from the required energy flux entering and exiting the ROx ($\dot{E}_7, \dot{E}_{10}$ respectively) determined by the specifications of the turbine. Particles are discharged from the HS to the ROx if the particle volume in hot storage is equal to greater than the particles required for electricity production.

The Ansaldo Energia AE64.3A gas turbine is used in the air Brayton model through a 1-D steady state quasi-equilibrium using Engineering Equation Solver (EES). From the model, the ROx output temperature, pressure and mass flow is specified [BRANDON]. Specifications for the power block were obtained from specification sheets provided by the manufacturer reference material and commercial gas turbine technical data for the 111.7 MW combine cycle (Turbomachinery Handbook 2015). The temperature out of the compressor (into the ROx) and into the turbine (out of the ROx) is 383 °C and 1200 °C, respectively. The nominal airflow rate is 213 kg/s. Remaining state values were determined through energy balances around each component with boundary conditions to meet the requirements for the power block.

Electrical power consumption for the vacuum pump is calculated from the oxygen flow and partial pressure. Electrical power consumption for the particle elevator is calculated from the particle flow and tower height.

The thermodynamic model is validated through its use in a previous investigation of a 111.7 MWh CSP system. The study reports the thermodynamic model development of the individual components, subsystem boundaries and the full system energy balance.

In the study the performance characteristics such capacity factor, system efficiency, spillage are calculated using the input DNI (Gorman et al. 2017). Some of the results from this work was used as inputs in the techno-economic analysis. The study referenced uses custom thermodynamic systems model that allows numerous parameters to be varied in a sensitivity analysis and connected to the cost performance analysis analyzed herein.

3.2 Thermodynamic Model Input Parameters

Table 2 provides input parameters for the thermodynamic equation set. The specific heat of the metal oxide CAM28 represents an average value observed from empirical study at the reduction temperature with the enthalpy of reduction approximated as a constant value from similar experimental analysis (Babiniec et al. 2016).

Table 2. Input Parameters for Simulated 111.7 MWe System

Component	Parameter	Value	Comments
Constants	Universal gas constant (R)	8.314 J/ mol×K	
	Ambient pressure (P_0)	101325 Pa	
Particles	Molar mass (M_p)	135.8 g/mol	Estimated based on specific material compositions (Commodity and Metal Prices n.d.)
	Average specific heat (c_p)	125.9 J/mol×K	Approximated as a constant independent of temperature and extent of reduction (Gorman et al. 2017)
	Extent of reduction (δ)	0.205	Result from the delta calculation at a required temperature of 1050°C and oxygen pressure of 200 Pa
	Packing density (ρ_p)	65%	Packing density of evenly sized sphere (The engineering Toolbox n. d.; Jaeger and Nagel 1992)
	Particle diameter (D_p)	0.25 mm	Material properties have been experimentally measured and characterized by Sandia National Laboratories (Babiniec et al. 2016)
	Volumetric density (v_m)	34.5 cm^3/mol	
SR3	Concentration factor (CF)	2,000,000	Engineering choice

	Emissivity (ε)	0.9	Based on the emissivity of black body efficiency and 0.8 for silica RSLE-57 (Schrader et al. 2015)
	Particle temperature out (T_4)	1050 °C	Engineering Choice
	Aperture area (A_a)	0.784 m^2	Result of total energy into the SR3 and a maximum aperture diameter of 1
	Number of receivers (N_{rec})	268	
	Area ratio (A_r)	24	Based on the apparatuses geometric configurations being worked at Sandia National Laboratories
	Oxygen partial pressure (P_{0_2})	200 Pa	Minimum practical working pressure for the vacuum pump
	Receiver rating (R_{rating})	420.7 MW	Result from the system mass and energy balance for the energy needed at state1
	Solar multiple (SM)	1.8	Yields the lowest LCOE with a storage capacity of 6 hrs
	Minimum operating irradiance (DNI_0)	350 W/m^2	This was decided in conservative estimations, as 300 is used elsewhere (Zhang et al. 2010)
HS	Ullage (V_{HS})	10%	Engineering assumption
	Storage hours (t_{st})	6 hr	DOE SunShot target
ROx	Number of pipes (N_{pip})	23	Numbers of pipes to suffice the particles flowing through the ROx, at a set pipe diameter.
	Packing density in ROx ($\rho_{p,rox}$)	5%	Engineering Assumption
HX	Heat transfer coefficient (U_{HX})	12 W/m^2	Value based gas-to-gas inside and outside tubes (The Engineering Toolbox n.d.)
Vacuum Pump	Pump electrical efficiency (η_{vp})	40%	The pump efficiency will depend on evacuated Pressure. Pumps are often unstable and inefficient at average and minimum conditions however can easily be optimized to higher efficiencies of > 60% (Ermanoski et al. 2013).
Power Block	Particle temperature in (T_{11})	1200 °C	Ansaldo Energia configuration from the AE64.3 gas turbine with a capacity of 75 MWe and a bottoming Rankine cycle for a total of 11.7 MWe
	Air mass flow ($\dot{m}_{air}$)	213 kg/s	
	Rated power (P_r)	111.7 MW	
	Compressor pressure ratio (p_r)	16.7:1	

	Thermal to electrical efficiency (η_{pb})	53.5%	
Solar Field	Solar field efficiency (η_{sf})	60%	Based on the actual efficiency range from 52% to 64% (Eddhibi et al. 2015; Ehrhart and Gill 2013).
Elevator	Height of lift (H_{lif})	135 m	A set parameter based on previous work (Gorman et al. 2017)
	Lift electrical efficiency (η_{lif})	80%	Based on value based on efficiency achieved by mine hoists (de la Vergne 2003)

The scaling parameter for each component and the particles is summarized in table 3. The total moles of particles in the system is calculated based on the number of particles required for six hours of off-sun production and a fraction of non-stored particles (F_{p}) of 10% as described in (3.3). The total area of the SR3 is dependent on the area ratio (A_{SR3}) between the external surface of the receiver and the area of the aperture(A_a), with three apertures per receiver. The volume of the hot storage is a direct function of the maximum number of moles stored $\left(\left[\dot{n}_p\right]_{7,10} \cdot t_{\mathrm{st}}\right)$ with an added ullage. The volume of the cold storage is estimated based on the remaining volume of particles remaining in the system. The solar field area is estimated based on a productivity of on-sun only generation and multiplied by a desired solar multiple. The geometry of the ROx is scaled as a function of the required pipe surface area. The pipe length, L_{pip}, is calculated based on the total time it takes for the particles to fully oxidize and for the air to reach the highest temperature before entering the power block. The pipe diameter, D_{pip}, is calculated based on the required cross sectional area of each pipe and is a function of particle mass and single particle property such as the density of the particles in the ROx, ρ_{rox}, and the particle packing density in the ROx, D_{p}. The surface area of one pipe is then multiplied by the number of pipes, N_{pip}. The

heat exchanger is scaled in respect to the heat transfer area, which is a function of the minimum heat capacitance of HX, C_{min}^{HX}, the number of transfer units for HX, NTU_{HX}, and the heat transfer coefficient, U_{HX}. Variables C_{min}^{HX} and NTU_{HX} are dependent on the energy balance and system temperatures to meet an effectiveness of 85%. The vacuum pump cost is based on the maximum power output from the pump to remove the oxygen from the SR3. The solar field area is based on a solar multiple, SM, and the required size of the field $A_{sf,n}$ for in-situ generation with no storage. The values are included for each parameter based on the inputs from table 2. The number of towers is dependent on the required number of receivers divided by 3 as there are 3 receivers per tower.

Table 3. Parameters Sizing Components

Component	**Scaling Parameter**	**Scaling Parameter Dependency**	**Value**
Particles	Mass of particles (m_p)	$m_p = M_p \cdot [\dot{n}_p]_{7,10} \cdot t_{\mathrm{st}} \cdot (F_{\mathrm{p}} + 1)$	5,147,328 kg
SR3	SR3 area (A_{SR3})	$A_{SR3} = A_r \cdot A_a$	7518 m2
Storage	Storage volume (V_{HS})	$V_{\mathrm{HS}} = \nu_m \cdot [\dot{n}_p]_{7,10} \cdot t_{\mathrm{st}}/(\rho_{\mathrm{p}} \cdot (1 + (U_{\mathrm{L}})$	2210 m2
ROx	ROx surface Area (A_{ROx})	$A_{\mathrm{rox}} = 2 \cdot \pi \cdot r_{pip} \cdot L_{pip} \cdot N_{pip}$	316 m2
HX	Heat transfer area (A_{HX})	$A_{HX} = NTU_{HX} \cdot C_{min}^{HX}/U_{HX}$	1042 m2
Vacuum Pump	Vacuum pump power ($\dot{E}_{16,m}$)	$\dot{E}_{16,m} = \max((n_{O2})_i \cdot R \cdot T_3 \cdot \log(p_{air}/p_{SR3}))/\eta_{pu}$	48.7 kW
Solar Field	Solar field area (A_{sf})	$A_{sf} = A_{sf,n} \cdot SM$	778,338 m2
Tower	Number of towers (N_{tow})	N_{tow}=N_{rec}/3	90

CHAPTER 4

COST MODEL DEVELOPMENT

Component sizes from the thermodynamic model are fed into the cost model to compute estimates of initial capital cost, operating and maintenance cost, and LCOE of the full-scale CSP system.

4.1 Cost Equations

Component costs are estimated using a scaling function with inputs including an independent variable (e.g., component size), a scaling function (e.g., linear relation), and a cost multiplier (e.g., installation costs). All costs vary according to a linear or power law scaling with respect to independent variables as indicated in Table 3. Multipliers account for added services or parts such as electrical, piping, fabrication, and installation.

The cost of each component is included in table 4 and uses the geometric scaling parameters from table 2 and cost multipliers.

Table 4. Scaling Parameters for Cost Calculations

Component	**Cost Equations**
Particles	$C_{pa} = m_{pa} \cdot M_{pa} \cdot C_{pa,i}$
SR3	$C_{SR3} = C_{m,r} \cdot F_{m,r} \cdot A_{SR3} \cdot N_{rec} \cdot (1 + P_s)$
Hot Storage	$C_{sH} = \left(\sum_{i=0}^{4} c_i\right) \cdot (1 + F_{c,misc}) + C_{ng}$
Lower Hopper	$C_{sLH} = A_{hs} \cdot C_{m,r} \cdot F_{SV} \cdot F_{m,r} \cdot (1 + P_s) \cdot F_{m,r}$
Upper Hopper	$C_{UH} = CF_{uh} \cdot C_{sLH} \cdot F_V$
ROx	$C_{ROx} = A_{ROX} \cdot C_{m,r} \cdot F_{m,r} \cdot (1 + P_s)$
HX	$C_{HX} = C_{hx,b} + C_{hx,a} \cdot A_{hx}$
Vacuum Pump	$C_{vp} = (Vp_0 + Vp_1 \cdot (\dot{E}_{16,m}/N_{rec}) \cdot (1 + P_s + M_e + Mu_p) \cdot N_{rec}$
Power Block	$C_{Pb} = F_{t,i} \cdot F_{t,c} \cdot P_R \cdot F_{t,p} \cdot (P_R{}^{F_{t,s}}(1 + P_s + M_e + Mu_p))$
Solar Field	$C_{SF} = A_{sf} \cdot (C_{sf})$
Tower	$C_{tower} = (1 + P_s + M_e) \cdot F_{ps} \cdot R_{rating}{}^{F_s}$
Elevator	$C_{elevator} = F_{se} \cdot R_{rating}$

The hot storage includes five layers of insulation where each layer is cost independently as illustrated in equation 4.1, where $V_0 = V_{hs}$.

$$c_i = (V_i - V_{i-1}) \cdot C_{ins,i} \tag{4.1}$$

Most installed cost of components, with exception to the power block and tower, scale linearly with the scaling parameters as illustrated in (4.2). The installed cost for each component is given as C_{com}, with C_{sp} as the scale parameter noted in Table 4, A_{sp} and B_{sp} are the fit constants and C_M is the total cost multipliers for each component ($C_M = 1 + multiplier$).

$$C_{com} = \left(A_{sp} + B_{sp} \cdot C_{sp}\right) \cdot C_M \tag{4.2}$$

The tower and the power block scale on a power law fit as demonstrated in (4.3).

$$C_{com} = A_{pf} \cdot B_{parameter}{}^{C_f} \cdot C_M \tag{4.3}$$

The total capital cost is based on the sum of the components and the cost of control given by $C_{control} = F_{control} \cdot \sum(C_{com})$ in addition to an owners cost a contingency as listed in (4.4).

$$C_{tca} = \sum(C_{com} + C_{control}) \cdot (1 + C_{own} + C_{con}) \tag{4.4}$$

The LCOE is estimated based on (3.7) in \$/kWh, where $C_{O\&M}$ is the total operation and maintenance cost per year, taking into account any parasitic losses of the plant, . The total capital cost, C_{tca}, is taken at a weighted average cost of capital per year, $wacc$, C_{rep} is the cost of material replacement per year, $C_{rep} = F_{rep} \cdot C_{pa}$,and E_p is the annual electrical production in kWh/year calculated in the model.

$$LCOE = \frac{C_{O\&M} + C_{tca} \cdot wacc + C_{rep}}{E_p} \quad (4.5)$$

4.2 Cost Model Input Parameters

Table 5 summarizes cost input parameters used to calculate total cost and LCOE of the CSP system. Values used are based on engineering understanding of plant design and referenced values when available. The last column of Table 5 justifies how each value is acquired. A sensitivity analysis was run to understand how changes in these assumptions can affect the total cost of energy.

Table 5. Cost Input Parameters for Simulated 111.7 MWe System

Component	Parameter	Value	Comments
Multiple	Setting percent (P_s)	20%	Estimate values for plant multipliers are obtained from the chemical engineering handbook of process design (Speight 2002)
	Electrical multiplier (M_e)	8.4%	
	Piping multiplier (Mu_p)	6.0%	
Particles	Particle cost (C_{pa})	\$1/kg	Based on the actual cost of production of the specific composition of the material (Commodity and Metal Prices n.d.)
	Particle multiplier (M_{pa})	2	Estimate to account for the fabrication of the particles
Solar Field	Cost field (C_{sf})	\$85/m^2	Based on the SunShot goal
ROx /Receiver	Material cost ($C_{m,r}$)	\$2400/m^2	Based on collaboration and communication with Hany Ansari (Ansari 2017).
	Material factor ($F_{m,r}$)	2.5	Estimate to account for the fabrication of the material
Tower	Pre-scaling factor (F_{ps})	26582	Based on a fit from existing installed CSP tower costs, where the cost varies with the receiver rating adjusted to 2015 (Sargent and Lundy 2003)
	Scaling factor (F_s)	0.95	

Storage	Nitrogen generator cost (C_{ng})	\$300,000	Based on actual costs of the materials of insulation and construction (Ho 2017).
	Compatibility layer cost ($c_{ins,0}$)	\$110,000/m^3	
	Insulating firebrick cost ($c_{ins,1}$)	\$11000/m^3	
	Perlite concrete cost ($c_{ins,2}$)	\$4700/m^3	
	Expansion board cost ($c_{ins,3}$)	\$5200/m^3	
	Reinforced concrete cost ($c_{ins,4}$)	\$1050/m^3	
	$F_{c,misc}$	5%	
	Upper and lower hopper volume ratio (F_{SV})	0.18	Estimate based on locating the majority of the particles in the bottom hopper
	Fraction of cold particles in the lower hopper (F_V)	85%	
Elevator	Elevator Scaling factor (F_{se})	2,600	Scaled based on the falling particle SunShot receiver adjusted to 2015 prices.
HX	HX Base cost ($C_{hx,b}$)	\$13,832	Both the vacuum pump and heat exchanger costs are scaled based on the process equipment estimation from DOE and adjusted to 2015 costs with CEPCI numbers (US Vacuum n.d.)
	Cost per area ($C_{hx,a}$)	\$185/m^2	
Vacuum Pump	Vacuum pump base cost (Vp_0)	\$4041	
	Vacuum pump scaling cost (Vp_1)	\$1600/kWh	
Power block	Turbine prefactor ($F_{t,p}$)	\$4,768/kW	Turbine factors are based on a power law fit from existing turbines of various rated powers and costs (Nye Thermodynamics Corporation n.d.)
	Turbine scale factor ($F_{t,s}$)	-0.260	
	Turbine installation factor ($F_{t,i}$)	2	
	Turbine complexity factor ($F_{t,c}$)	1.35	
Balance of Plant	Owners fraction (F_{own})	17%	Costs are based on System Advisor Model (SAM) (NREL/TP -5500-57625 2013). Parameters are taken at the same value as SAM, or at a more conservative value to account for any additional uncertainties of the technology.
	Weighted average cost of capital ($wacc$)	8%/year	
	Fraction of particle replacement (F_{rep})	10%/year	
	Contingency (C_{con})	25%	
	Yearly cost of operation (C_{omi})	\$40/kWe-yr	SunShot standard

4.3 Cost Model Validation

To validate the methods of the model, the data was used in estimating the actual power plant, Ivanpah, on our methods (Table 6). The cost of Ivanpah was estimated based on the Molten Salt Power Tower Cost for Modeling with the System Advisor Model (SAM), (NREL/TP -5500-57625 2013) and associated spreadsheet. The resulting cost estimate of $2.06B is 6.4% less than the stated cost of $2.2B.

Table 6. Estimated Cost of a Single Ivanpah Tower and the Combined Three Towers Based on the NREL Methodology

Direct capital cost summary	**Single tower Ivanpah**	**Ivanpah estimated cost**	**For full plant Ivanpah**
Site improvements	$75,741,300.00	$ 16.00	$ 22,623,900.00
Heliostat field	$159,031,796.00	$181.00	$ 477,095,388.00
Tower	$16,763,508.00	$32.00	$50,290,525.00
Receiver	$98,780,752.00	$185.00	$296,342,257.00
Thermal energy storage		$26.00	
Balance of plant	$45,155,878.00	$346.00	$135,467,633.00
Power plant	$152,900,881.00	$ 1,170.00	$458,702,644.00
Contingency	$ 38,372,188.00	$ 7.00	$115,116,564.00
Total Direct Costs	$586,546,304.00		$1,759,638,912.00
Indirect capital cost summary			
EPC and owners costs	$64,519,654.00	11%	$193,558,961.00
Land	$10,180,000.00	$ 10,000.00	$30,540,000.00
DC's sales tax	$25,391,572.00	4%	$76,174,717.00
Total installed costs	$686,637,530.00		$2,059,912,590.00
Mirror area (m^2)	877,910.00		2633730
Tower heigh (m)	140		
Receiver thermal (MWth)	535		1,605
Thermal storage (MWh)	0		0
Rated power (Mwe)	137.67		392
Hours storage (hrs)	0		

CHAPTER 5

SIMULATION METHODS

This study uses a three step procedure to analyze the LCOE of the CSP plant as illustrated in Fig 3. A design point analysis is first conducted to calculate required size of each component described previously. Productivity analysis follows to equate plant generation over a one-year period using hourly DNI data. Simulation concludes with a financial analysis to equate the LCOE using equipment sizes and productivty from prior steps. Independent parameters for each step are varied during sensitivity analysis to examine effect on productivity, cost, and LCOE. The thermodynamic and financial models were written in Python.

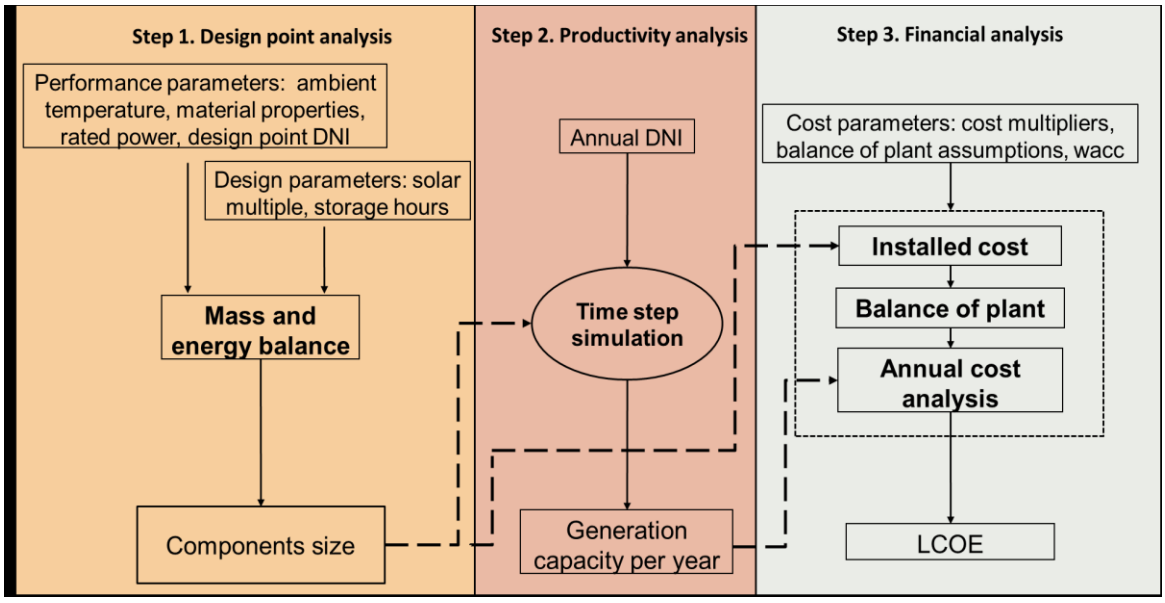

Figure 3. Computational Procedure for Performance and Costing Analysis

Step 1: Component Sizing: Performance and design parameters are put in to the model for a full system mass. Here the thermodynamic performance parameters such as ambient temperature, material properties, rated power and design point DNI are input into

the mass and energy balance. An initial energy balance is performed to determine the size of the solar field to reflect sufficient radiation for the generation based on the established rated power and no storage. The design parameters such as the solar multiple and storage hours are input to establish the scale up of the system. The full mass and energy balance determines the number of particles that need to be both stored and used in heat exchange which is used to size of the SR3, HS, ROx, CS, HX, and vacuum pump.

Step 2: Performance Simulation: A quasi-steady state thermodynamic equation set permits simulation of CSP operation using hourly time steps for a representative year (1988) maintained by the national renewable energy laboratory (NREL). The model uses the hourly annual DNI from the specific location, along with the calculated component geometry to calculate the total generation capacity per year. The model can be used to predict the performance of this plant in different geographic locations with different annual DNI. The energy input at each time step determines if there is generation. If the DNI is higher than the cut off DNI, and there are sufficient particles in the hot storage to be released into the ROx, there is generation. The amount of particles radiated to be stored in the hot storage is limited by the size of the hopper determined from Step 1. The sum of the hours at the end of the look is the generation capacity per year.

Step 3: Cost Analysis: The installed cost is calculated using the cost parameters and component geometries from the design point analysis followed by a balance of plant and adjusted cost per year. First the cost multipliers, are used in combination with the components size from Step 1 to calculate individual component cost. The summation of the component costs results in the installed cost. Using balance of plant independent assumed inputs, the balance of plant is calculated. Finally the total yearly cost is normalized

with the generation capacity per year, calculated in Step 2 to result in an LCOE. Because of the interdependence of the 3 Steps, a variation in any of the independent inputs will affect the LCOE.

CHAPTER 6

RESULTS FOR BASELINE SYSTEM

Figure 4 illustrates installed cost of component estimated from thermodynamics and costing multipliers from Table 2 and Table 5 respectively. The generation is calculated from the sun of the generation per hour for one full year. The total installed cost, total capital cost, cost of capital payments per year, cost of particle replacement and operation and maintenance costs are listed followed by the LCOE estimated at $0.071/kWh.

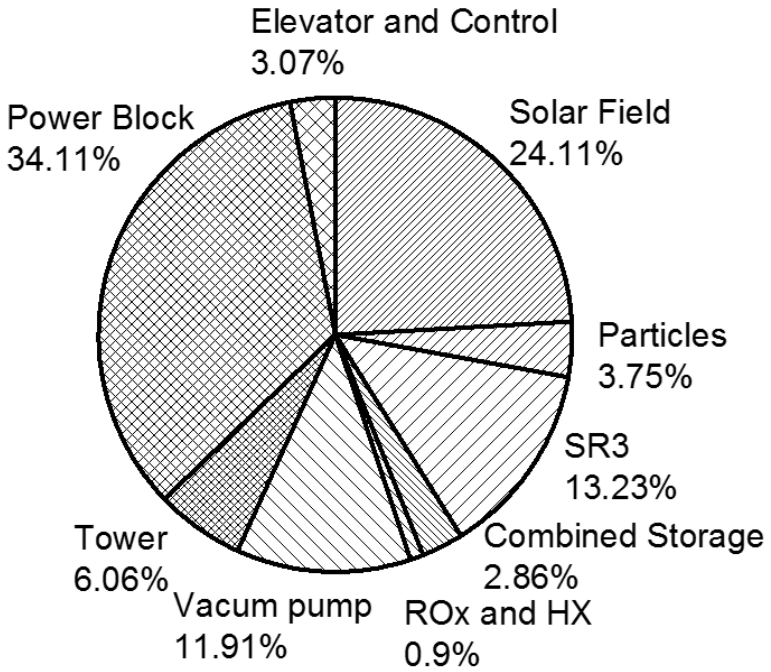

Total Installed Cost	$274,396,108
Total Capital Cost	**$408,706,916**
Total Capital Cost per year	**$32,696,553**
Particle Replacement	**$1,029,465**
Operation and Maintenance	**$2,313,567**
Generation Capacity	507 GWh/yr
LCOE ($/kWh)	0.071

Figure 4. Effect of Each Component on the Total Installed Cost and Calculated Values for LCOE Analysis with Base Line Parameters (Tables 2 and 4).

The majority of system cost comes from the Power Block followed by the Solar Field, as expected. The cost of the Power Block is estimated based on the scaling equations. In the designed system, a commercial Power Block combustor is replaced by the ROx, in which the particles undergo an exothermic reaction and exchange heat with

compressed air. This figure baselines this technology against current CSP and in pinpointing target areas to focus on improving. It is technologically difficult to reduce the cost of the power block and the solar field, since the current analysis already assumes DOE SunShot goals for the solar field and market prices for the power block. Reduction in the SR3, ROx and vacuum pump can be analyzed and provide a high reduction in the total cost.

The majority of system cost comes from the Power Block followed by the Solar Field, as expected. The cost of the Power Block is estimated based on the scaling equations. In the designed system, a commercial Power Block combustor is replaced by the ROx, in which the particles undergo an exothermic reaction and exchange heat with compressed air. This figure baselines this technology against current CSP and in pinpointing target areas to focus on improving. It is technologically difficult to reduce the cost of the power block and the solar field, since the current analysis already assumes DOE SunShot goals for the solar field and market prices for the power block. Reduction in the SR3, ROx and vacuum pump can be analyzed and provide a high reduction in the total cost.

Through nature of the SR3 being an innovative component of this technology, it presents unknown parameters. There is a high level of uncertainty on both the performance and cost parameters and therefore an opportunity to drive down the cost with increased manufacturing. Sensitivity on these parameters allow for a better idea on how to target the component design to minimize the LCOE. The ROx has a consistent pipe flow design with many of its parameters resulting from the thermodynamics of the remainder of the system. In this model, the opportunity in cost reduction of this component is in the material cost

multiplier. The vacuum pump is an existing technology with an opportunity in the design of the component for specific load to maximize the efficiency.

CHAPTER 7

SENSITIVITY ANALYSIS

Specific parameters have large varying levels of impacts on individual components and the system as a whole. Sensitivity analysis was performed to analyze the influence of performance, costing and design parameters on the overall installed cost, generation capacity and levelized cost of energy of the proposed CSP system. Engineering parameters include the SR3 area ratio between the aperture and the reactor cavity, the heat transfer coefficient for the heat exchanger NTU calculation, the packing density of the particles used in sizing and heat transfer calculation for the storage hoppers, the pump efficiency for SR3 oxygen evacuation, and the cut-off DNI that determines the minimal solar radiation necessary to begin operation. The costing parameters include the setting percent, a chemical engineering design standard for calculating full plant installation costs, wacc, which estimates how much of the total cost is payed per year, SR3 multiplier, used to estimate the SR3 material cost, the contingency, for unexpected costs associated with the construction of the plant, and the particle cost multiplier for cost associated with manufacturing the particles out of the bulk material. The design parameters including solar multiple and storage hours have a non-linear high impact on the LCOE and were investigated from a solar multiple of 1.2 to 2.8 and storage hours between 4 and 14 hours. Model results seek to size component and conduct both component and cost analysis to meet a LCOE of under $0.06 US cents/kWh.

7.1 Influence of Performance Parameters

Changes to performance properties of the material could impact the size of various components. Figure 5 illustrates the design, minimum and maximum value for each sensitivity variable used in the analysis. Figure 5 represents the results of a simulation on the installed cost, generation and LCOE when each parameter is varied independently. The relative influence of each component is represented as positive, negative or negligible (<0.01%) change from the design value. If an increase in value results in an increase of the metric being analyzed, the change is positive. If an increase in variable value results in a decrease in the metric being analyzed the relation is negative. If there is no, or minimal effect of changing the variable on the component being analyzed, the relation is negligible. The influence of each variable is summarized in the discussion that follows.

SR3 area ratio: An increase in the SR3 area ratio results in an increase on the total area of the SR3. As illustrated by Fig. 5, the SR3 area ratio has the largest influence on the LCOE due to its large effect on cost. A smaller SR3 area ratio would minimize the thermal losses and cost, however it is limited by the angle of the apparatus and its distance to the receiver. Because this is a new component there is a lot of uncertainty with the area ratio, therefore a sensitivity allows an understanding on how this parameter can affect the LCOE. Although the generation does not change, an increase in loss in the SR3 due to the increase in surface area results in a larger solar field area needed to assure meet the required radiation into the particles.

Heat transfer coefficient: A NTU method of calculating heat transfer is used to size the effective heat exchange area with an effectiveness of 85%. The heat transfer coefficient has a positive relation to the generation as it increases thermal energy going into the SR3,

and a negligible relation with cost. Increasing the heat transfer coefficient decreased the overall LCOE by 0.12%.

Particle packing density: The packing density of the particle in the hot storage influences the mass of particles required in the system. Randomly packed particles with a uniform diameter have a packing density of 65% as chosen by the design. However this is an uncertainty and presents an opportunity for cost reduction, as the material of choice will not be uniform in diameter. This parameter is limited by physical properties of the manufactured particle. An increase in packing density increases the energy density and decreases sizing of the hot storage, and the cost of particles. A decrease to the packing density to 50% decreases the LCOE by 0.38%.

Pump efficiency: The pump efficiency is highly dependent on the operation based on its design point. A pump operating at design point conditions can reach higher than 80% efficiency. This variable offers high opportunity in cost reduction as an increase in efficiency decreases cost. In this model parasitic loses are accounted for in the cost of operation and maintenance. The change to the generation is negligible, however the lowered parasitic losses due to high energetic efficiency decreases both the vacuum pump cost and the total balance of plant. The LCOE decreased by 3.42% when the efficiency was raised to 60%.

Cut-off DNI: The cut-off DNI is the point which the elevator begins pulling particles through to the SR3. Lowering this parameter allows for the system to work longer during the day, at times where the solar radiation is not as strong. A decrease in the cut-off DNI increases the generation of the CSP plant. What limits this parameter is whether there is enough flux after re-radiation to heat and reduce the particles to the target

temperature/reduction extent. The extent of which generation is increased or decreased is dependent on the quantity of lower level (early or late in the day) radiation available.

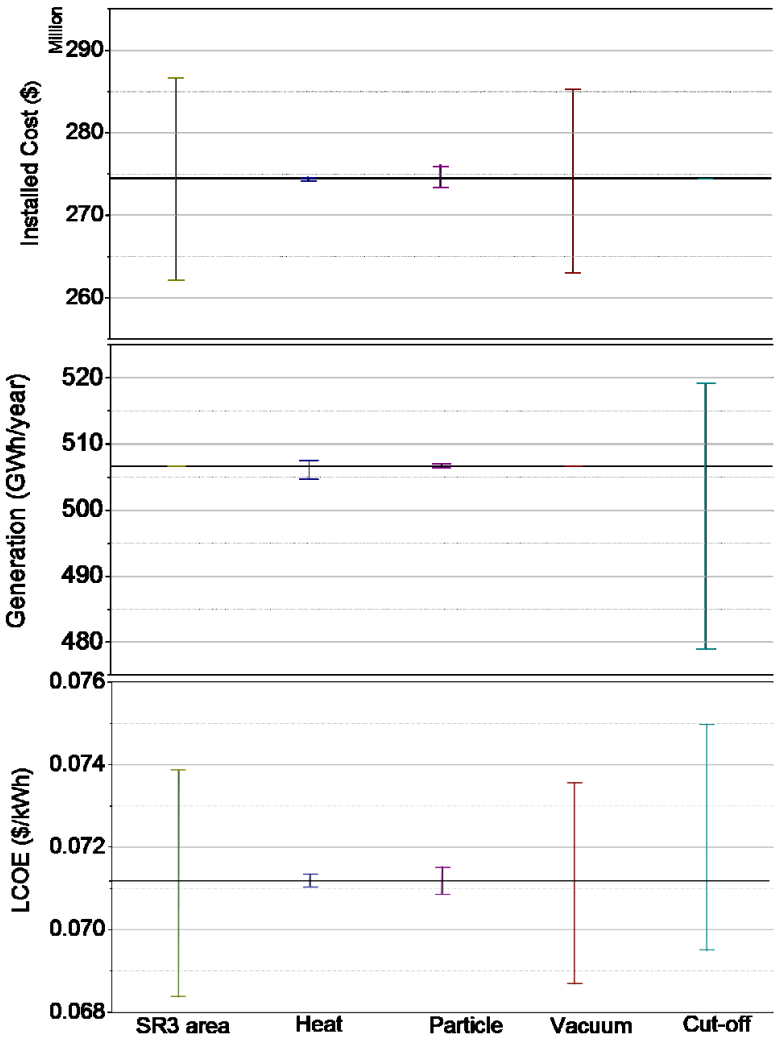

	Value			% Change		
	Minimum	Design	Maximum	Generation	Installed Cost	LCOE
SR3 area ratio	16	24	32	Negligible	+ 4.46%	+ 5.06%
Heat transfer coefficient	4 W/m²	12 W/m²	20 W/m²	+ 0.18%	Negligible	- 0.12%
Particle packing density	50%	65%	80%	Negligible	- 0.37%	- 0.38%
Pump efficiency	50%	40%	60%	Negligible	- 3.96%	- 4.12%
Cut-Off DNI	200 W/m²	350 W/m²	500 W/m²	- 4.24%	Negligible	+ 3.82%

Figure 5. Sensitivity Analysis of Sizing Parameters and Cost Multipliers. Graphs Correspond to Parameter Effects on (A) Total Cost, (B) Plant Generation, (C) Levelized Cost of Energy

7.2 Influence of Cost Parameters

Changes to cost parameters of the particles impacts the cost of the plant and therefore the LCOE. Cost parameters do not affect the thermodynamic performance of the system and therefore do not influence the generation capacity of this CSP plant. The linear impact on the LCOE of five cost parameters are analysed in Fig. 6. The design values of each parameter results in an LCOE of $.071/kWh. The minimum, maximum and design values are listed and all of the parameters analysed have a positive relation to the LCOE.

wacc: The wacc demonstrates the largest impact on the LCOE, with a 1% change. It effects the LCOE by 11.3%. Currently a wacc of 7.5% is reasonable for countries where borrowing money is relatively low and stable, but can be as high as 10% in various other parts of the world (IRENA 2015). The wacc presumes that there is both debt and equity on the plant. A sensitivity was performed on the 8% assumed wacc to understand the extent of influence it has on a 1% change. There is a high negative relation to the LCOE as decreasing the wacc means lower annual payments.

SR3 multiplier: The SR3 effects > 13% of the installed costs (Fig. 4) and provides an opportunity in the total cost reduction. There are various uncertainties associated with this novel reactor, therefore sensitivity allows analysis on the importance of the material cost on the LCOE.

Contingency: The contingency is a cost parameter used to account for any unpredicted cost. A 25% design value is as a conservative value. This value can be decreased if it is being built in a predictable area such as one of low natural disasters, or political turmoil. A 5% change on this parameter has a positive 3.1% change on the LCOE.

Particle multiplier: The redox-active metal oxide used in this CSP contains various uncertainties in both performance and cost. A sensitivity analysis reduces the uncertainties on how the cost will affect the LCOE of the plant. The particle multiplier is used to predict an added cost of fabrication of the particles from bulk material. The particles account for both a >3.0% of the total installed cost, and the yearly particle replacement cost. A 40% change in the material multiplier effects the LCOE by 1.5%.

Setting Percent: The setting percent is the added installation cost associated with the CSP plant. As illustrated a decrease on these installation costs of 5%, can reduce the LCOE by 2.3%.

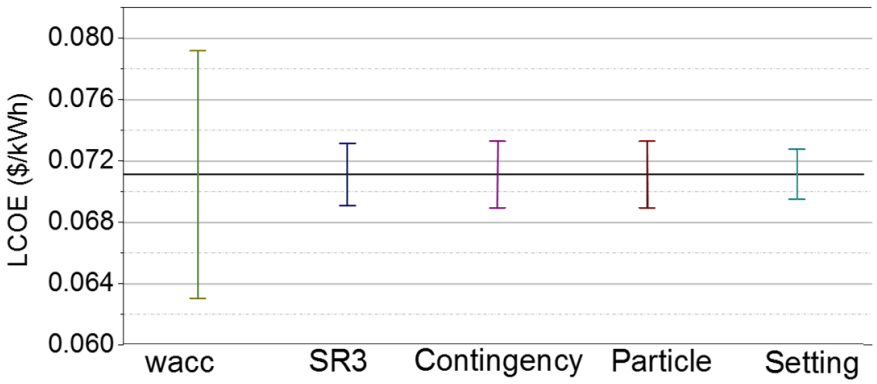

	Value			
	Minimum	**Design**	**Maximum**	**% Change**
wacc	7%	8%	9%	+ 11.3%
SR3 multiplier	2	2.5	3	+ 2.9%
Contingency	20%	25%	30%	+ 3.1%
Particle multiplier	1.5	2	2.5	+ 1.5%
Setting %	15%	20%	25%	+ 2.3%

Figure 6. Sensitivity Analysis of Sizing Parameters and Cost Multipliers and the Effect on the LCOE

7.3 Influence of Design Parameters

Two design parameters that have a significant effect on LCOE are the solar multiple and storage capacity of a CSP. Figure 7 demonstrates the effects of both of these parameters on the total plant cost, the generation capacity and finally the LCOE of the plant. The parameters were analyzed for solar multiple from 1 to 2.8 and TES from 4 to 14.

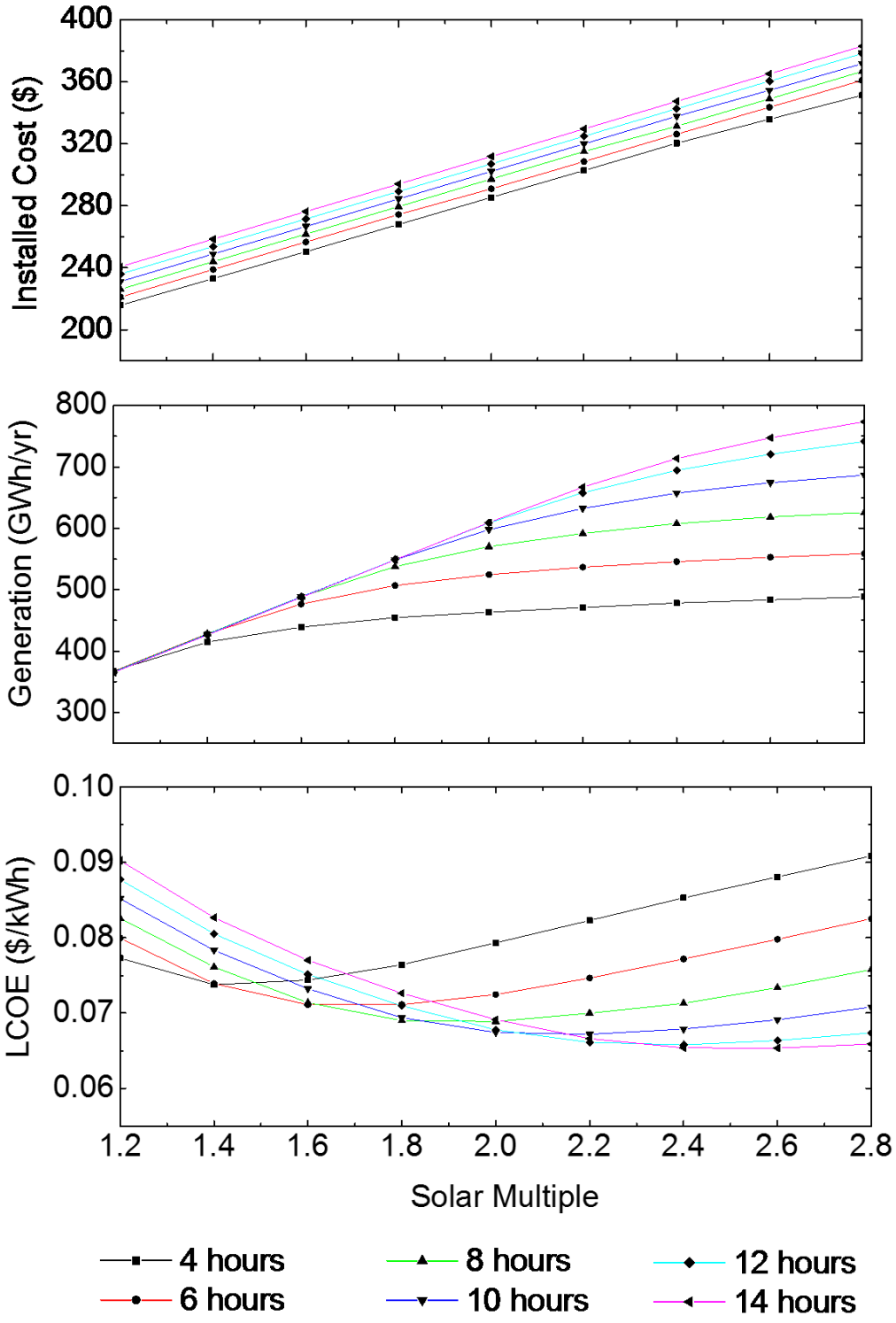

Figure 7. Effect of Storage Capacity and Solar Multiple on the (a) Installed Cost, (b) Generation Capacity, and (c) LCOE.

The linear increase of the plant cost illustrates that both parameters have a positive linear relation with the cost of the plant. As expected, at low solar multiples, the solar multiple is the limiting factor, and increasing the storage capacity does not increase generation. At high solar multiples, the storage capacity is the limiting factor, as the plant can only generate electricity if there are sufficient hopper space to hold the particles that store energy during sun-off hours. The linear increase of the cost accompanied by a limit in generation creates a minimum in the LCOE represented by Fig. 7c. The ideal combination of solar multiple and energy storage capacity is illustrated by the "perceived minimum LCOE." Various CSP plants built in the last few years use a storage capacity of 6 hours which results in a 1.8 solar multiple. Larger storage capacity and optimal solar multiples should be considered as they result in lower LCOE.

7.4 Approaching LCOE Targets

Various parameters present opportunity to reach a LCOE below $0.06/kWh. For this demonstration illustrated in Fig. 8 the solar multiple, hot storage, cut-off DNI, pump efficiency and setting percent where analyzed, followed by the contingency and wacc. The parameters where selected based on their individual impact to the total plant LCOE (Fig. 6 and 7) and their feasibility to be changed based on current technological and financial knowledge. A solar multiple of 2.2 was chosen for 12 hours of storage capacity based on the minimum LCOE of 12 hours (Fig. 7). A cut-off of 200 W/m^2 DNI is chosen to increase the hours that the generation of the system without increasing cost. The pump efficiency was raised from 40% to 60% as it can range based on the oxygen flow and performance. The contingency was decreased to a less conservative 20% and the wacc was lowered to 7%.

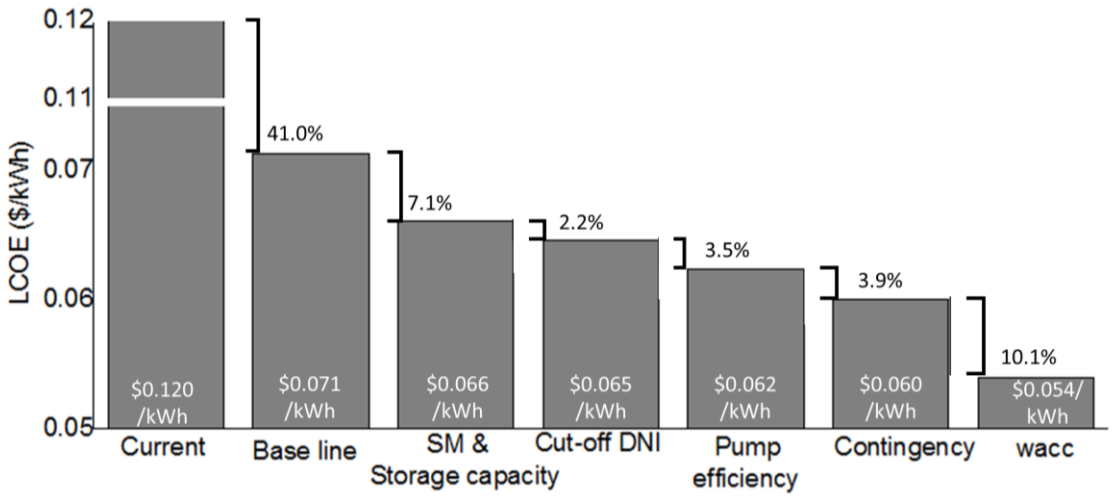

Figure 8. Scenario Where LCOE Reaches Lower Than the Target $0.06/kWh by Cumulative Variation of Design, Performance and Cost Parameters

The baseline case falls 41.0% below the current LCOE for CSP plants, and shows potential to reduce significantly more with adjustment to other parameters. There is significant study on the impact of a higher solar multiple and storage capacity on the decrease of the LCOE. The LCOE reached $0.066/kWh when solar multiple of 2.2 and storage capacity of 14 hours was used. The cut-off is a design choice and was modified following the sensitivity analysis (figure 5). The decrease to 200 W/m^2 increased the generation by 15.75 GWh and lowered the LCOE by an additional 2.2% to $0.065/kWh. Increasing the pump efficiency to 60%, resulted in a LCOE of $0.062/kWh. The decrease in the contingency brought the value to $0.060/kWh, hitting the DOE SunShot target. A further analysis on the impact of a 1% lower wacc resulted in a LCOE of $0.054/kWh.

CHAPTER 8

DISCUSSION

This study illustrated an alternative to high-cost, nonrenewable, and unreliable grid power by introducing a TCES system with a novel CSP plant design. The analysis suggests that the proposed CSP plant in this study could provide low-cost power to obtain grid-parity with other forms of power generation and thereby reduce impact on the environment from fossil fuel use. The study demonstrates a decrease from the current $0.12/kWh of unsubsidized LCOE to the $0.071/kWh illustrated by the base line analysis. The technology has potential to be cost effective, taking advantage of a high efficiency storage and power block that requires a higher temperature heat exchange fluid than traditional technologies. Sensitivity analysis is performed on cost and performance parameters to illustrate how they affect total cost of electricity to meet the DOE SunShot near-term (2020) goal of $0.06/kWh. A cumulative parameter analysis demonstrates one scenario of the LCOE reaching bellow the target goal. A combination of sensitivity on any additional high impact variable would lead to the same or lower LCOE.

The majority of CSP plants have a storage capacity of six hours due to high cost of capital and no added value for the added capacity. The investment of higher storage capacity is advantageous as it can lead to significant decreases in LCOE, especially with increasing solar multiple. However, because LCOE is not the only financial consideration when building a CSP plant, both performance and cost parameters must also be understood. Research in materials of heat transfer, insulation and construction continue to decrease the individual components cost. As research continues on new components (SR3 and ROx) increase in efficiencies and decrease in cost of material production will facilitate

the DOE SunShot goal to be surpassed. As policy and regulation minimizes perceived risk for CSP plants, the wacc can be reduced which will then reduce the LCOE (International Renewable Energy Agency 2014). More design and modeling work allows various uncertainties from these components to be eliminated through prediction on parameter impact to the LCOE.

REFERENCES

Ansaldo Energia. (2013). AE64.3A Gas Turbine. Retrieved from: http://ansaldoenergia.it/easyUp/file/gas_turbine_ae64_3a_june2013.pdf

Ansari, H. A. (2017). Personal communication.

Babiniec, S. M., Coker, E. N., Miller, J. E., Ambrosini, A. (2016). *International Journal of Energy Research*, 40(2), 591-610.

Boekhoudt, A., Behrendt, L. (2014). Taxes and incentives for renewable energy. KPMG International.

Boudaoud, S. A., Khellaf, Mohammedi, K., Behar, O. (2015). Thermal Performance Prediction and Sensitivity Analysis for Future Deployment of Molten Salt Cavity Receiver Solar Power Plants in Algeria. *Energy Conversion and Management* 89(02): 655–64.

Boucher, R., Rodzianko, P. (1994). Advanced Pumped Storage: The New Competitive Edge. *The Electricity Journal*. 7(6), 27-37.

California ISO. (2013). Demand response and energy efficiency roadmap: Maximizing preferred resources. California ISO, USA.

Charles, R. P., Kenneth, W. D., L Smith, J. L. (2005). Assessment of Concentrating Solar Power Technology Cost and Performance Forecasts. *Electric Power 2005*: 1–25.

Commodity and Metal Prices. (n.d.). *InfoMines.* [Online data]. Retrieved from: http://www.infomine.com/investment/

De la Vergne J. (2003). Hard Rock Miner's Handbook, 3rd Ed. McIntosh Engineering Limited. Tempe, AZ, 215.

Duke Solar Energy (2001). Subtask 1.2 Final Report, A Non-Imaging Secondary Reflector for Parabolic Trough Concentrators. NREL Subcontract No. NAA-1-30441-06. Golden, CO: National Renewable Energy Laboratory

Durkay, J. (2016). State renewable portfolio standards and goals. *National Conference on State Legislatures*.

Eber, K., Corbus, D. (2013). Hawaii solar integration study: executive summary. National Renewable Energy Laboratory.

Eddhibi, F., Amara, M. B., Balghouthi, M., Guizani, A. (2015). Optical study of solar tower power plants. *Journal of Physics*: Conference Series, 596, 012018.

Ehrhart, B., Gill, D. (2013). Evaluation of annual efficiencies of high temperature central receiver concentrated solar power plants with thermal energy storage.

Energy Policy Act. (2005). 109th Congress Public Law. U.S. Government Printing Office.

Ermanoski, I., Siegel, N. P., Stechel, E. B. (2013). A New Reactor Concept for Efficient Solar-Thermochemical Fuel Production. *Journal of Solar Energy Engineering. 135(3), 031002.*

Garg, H.P. et al. (1985). Solar Thermal Energy Storage, D. Reidel Publishing Company, Dordrecht/Boston/Lancaster. ISBN 90-277-1930-6.

Germany Federal Ministry for Economic Affairs and Energy. 2014. An electricity market for German's energy transition. Federal Ministry for Economic Affairs and Energy, Germany.

Glatzmaier, G. (2011). Summary Report for Concentrating Solar Power Thermal Storage Workshop: New Concepts and Materials for Thermal Energy Storage and HeatTransfer Fluids.

Gorman, B. T., Johnson, N. G., Miller, J. E., Stechel E. B. (2017). A Steady State Thermodynamic Model of Concentrating Solar Power with Thermochemical Energy Storage. In Review.

Ho, C. (2017). Personal communication.

International Renewable Energy Agency (IRENA). (2014) Renewable Power Generation Costs in 2014. Renewable power generation costs (2014): 1–8. Print.

International Renewable Energy Agency. (2015). Renewable Power Generation Costs in 2014 : An Overview." *Irena Homepage* (January): 92

Jamehbozorg, A., Keshmiri, S. N., Radman, G. (2011). PV output power smoothing using energy capacitor system. *Proceedings of 2011 IEEE Southeastcon*.

Janko, S. A., Arnold, M. R., Johnson, N. G. (2016). Implications of high-penetration renewables for ratepayers and utilities in the residential solar photovoltaic (PV) market. *Applied Energy*, *180*, 37-51.

Jaeger, H. M., Nagel, S. R. (1992). Physics of the Granular State. Science, 255(5051), 1523–1531.

Jorgenson, J., Mark M., and Paul D. (2016). "Comparing the Net Cost of CSP-TES to PV Deployed with Battery Storage." *AIP Conference Proceedings* 1734.

Lam, R. K., Yeh, H. G. (2014). PV ramp limiting controls with adaptive smoothing filter through a battery energy storage system. *Proceedings of 2014 IEEE Green Energy and Systems Conference*.

Lieurance, D., Kimball, F., Rix, C. (1995) "Design and Cost Studies for Small Scale Superconducting Magnetic Energy Storage (SMES) Systems," IEEE Transactions on Applied Superconductivity, Vol. 5, No. 2, pp. 350-353.

Lorenzin, N., Abánades, A. (2016). A review on the application of liquid metals as heat transfer fluid in Concentrated Solar Power technologies. *International Journal of Hydrogen Energy*, 41(17) 6990-6995.

Miller, J., Ambrosini, A., Coker, E., Allendorf, M., McDaniel, A. (2014) Advancing Oxide Materials for Thermochemical Production of Solar Fuels. *Energy Procedia 49*. 2019-26.

National Renewable Energy Laboratory. (n.d.). National Solar Radiation Data Base [CSV data file]. Retrieved from http://rredc.nrel.gov/solar/old_data/nsrdb/1991-2005/tmy3/by_state_and_city.html

Nye Thermodynamics Corporation. (n.d.) Retrieved from: www.gas-turbines.com/trader/kwprice.htm.

Pacio, J., Wetzel, T. (2013). Assessment of liquid metal technology status and research paths for their use as efficient heat transfer fluids in solar central receiver systems. *Solar Energy*, 93 11-22.

Pardo, P., Deydier, A., Anxionnaz-Minvielle, Z., Rougé. S.,Cabassud, M., Cognet, P. (2014). A review on high temperature thermochemical heat energy storage." *Renewable and Sustainable Energy Reviews*. 32, 591-610.

Pena, M. A., Fierro., J. L. G. (2001). Chemical structures and performance of perovskite oxides. *Chemical Reviews.* 101(7), 1981-2018.

Price, H. (2001) Concentrated Solar Power Use in Africa. NREL/TP. Golden, CO: National Renewable Energy Laboratory.

Price, H. (1997). Guidelines for Reporting Parabolic Trough Solar Electric System Performance. NREL/CP-550-22729. Golden, CO: National Renewable Energy Laboratory.

Price, H. (2000). "UVAC Test HCE Heat Loss Model" Excel Spreadsheet. Golden, CO: National Renewable Energy Laboratory.

Sargent and Lundy. (2003) Assessment of Parabolic Trough and Power Tower Solar Technology Cost and Performance Forecasts. National Renewable Energy Laboratories

Sawin, J. L., Seyboth K. M., Sverrison F., Adib R. (2016). Renewables 2016-Global Status Report.

Schrader, A. J., Muroyama, A. P., Loutzenhiser, P. G. (2015). Solar electricity via an Air Brayton cycle with an integrated two-step thermochemical cycle for heat storage based on Co3O4/CoO redox reactions: Thermodynamic analysis. Solar Energy, 118, 485–495.

Shabgard, H., Faghri, A., Bergman, T. L., Andraka, C. E. (2014). Numerical Simulation of Heat Pipe-Assisted Latent Heat Thermal Energy Storage Unit for Dish-Stirling Systems. *Journal of Solar Energy Engineering*. 136(2), 21-25.

Sharifi, N., Faghri, A., Bergman, T. L., & Andraka, C. E. (2015). Simulation of heat pipe-assisted latent heat thermal energy storage with simultaneous charging and discharging. *International Journal of Heat and Mass Transfer,* 80, 170–179.

Speight, J. G. (2002). Chemical Process and Design Handbook. McGraw-Hill. Print.

The Engineering Toolbox. (n.d.). Drag Coefficient [Online data table]. Retrieved from http://www.engineeringtoolbox.com/drag-coefficient-d_627.html

The Engineering Toolbox. (n.d.). Heat Exchanger Heat Transfer Coefficients [Online data table]. Retrieved from http://www.engineeringtoolbox.com/heat-transfercoefficients-exchangers-d_450.html

Thomas, A.; Guven, H. M. (1993). "Parabolic Trough Concentrators – Design, Construction and Evaluation." Energy Conversion Management (34:5); pp. 401–416.

Thongpron, J., Sangpanich, U., Limsakul, C., Chenvidya, D., Kirtikara, K., Jivacate, C. (2004). Study of a PV-grid connected system on its output harmonics and voltage variation. *Asian Journal on Energy and Environment*, *5*(1), 59-73.

Turbomachinery Handbook 2015, Power Engineering International.

U.S. Department of Energy. (2009). High penetration of photovoltaic (PV) systems into the distribution grid. U.S. Department of Energy.

U.S. Department of Energy. (2015b). Quadrennial technology report 2015.

U.S. Energy Information Administration. (2016). Annual Energy Outlook 2016 with projections to 2040. Washington DC: U.S. Retrieved from https://www.eia.gov/outlooks/aeo/pdf/0383(2016).pdf

U.S. Federal Energy Regulatory Commission. (2012). Integration of variable energy resources. Docket No. RM10-11-000, Order No. 764. USA Federal Energy Regulatory Commission.

US Vacuum. (n.d.). Retrieved from: www.usvacuumpumps.com.

Wang, G., Ciobotaru, M., Agelidis, V. G. (2014). Power smoothing of large solar PV plant using hybrid energy storage. *IEEE Transactions on Sustainable Energy*, *5*(3), 834-842.

Wirth, H. 2015. Recent facts about photovoltaics in Germany. Fraunhofer Institute for Solar Energy Systems.

World Energy Council. (2010). Survey of energy resources. Retrieved from: https://www.iea.org/publications/freepublications/publication/WorldEnergyOutlook2016ExecutiveSummaryEnglish.pdf

World Energy Outlook. (2016). *International Energy Agency.*

Zhang, Y., Smith, S. J., Kyle, G. P., Stackhouse, P. W. (2010). Modeling the potential for thermal concentrating solar power technologies. Energy Policy, 38(12), 7884–7897.